Biosensors and Bioelectronics 78 (2016) 31–36

Contents lists available at ScienceDirect

Biosensors and Bioelectronics

journal homepage: www.elsevier.com/locate/bios

A novel biosensor for *Escherichia coli* O157:H7 based on fluorescein-releasable biolabels

Rong-Rong Hu [a,b], Zheng-Zhi Yin [b,*], Yan-Bo Zeng [b], Jian Zhang [b], Hai-Qing Liu [b], Yong Shao [c], Shi-Bin Ren [d], Lei Li [a,b,**]

[a] College of Petrochemical Engineering, Changzhou University, Changzhou 213614, PR China
[b] College of Biological, Chemical Sciences and Engineering, Jiaxing University, Jiaxing 314001, Zhejiang Province, PR China
[c] College of Chemistry and Life Sciences, Zhejiang Normal University, Jinhua 321004, PR China
[d] School of Chemistry and Chemical Engineering, Nanjing University, Nanjing 210093, PR China

ARTICLE INFO

Article history:
Received 30 July 2015
Received in revised form
5 November 2015
Accepted 8 November 2015
Available online 10 November 2015

Keywords:
Fluorescein-releasable biolabel
Magnetic separation
Escherichia coli O157:H7
Biosensor

ABSTRACT

New techniques are required for the rapid and sensitive detection of *Escherichia coli* O157:H7 (*E. coli* O157:H7), a pathogenic bacterium responsible for serious and sometimes life-threatening diseases in humans. In this study, we developed a highly sensitive and efficient biosensor for the quantitative detection of *E. coli* O157:H7 by integrating fluorescein-releasable biolabels with a magnetism-separable probe. Hollow silica nanospheres with a diameter of approximately 350 nm were synthesized, enriched with fluorescein, and surface-protected with macromolecule layers of poly (acrylic acid) and poly (dimethyldiallylammonium chloride). These fluorescein-enriched hollow silica nanospheres were characterized using scanning electron microscopy, transmission electron microscopy, and Fourier transform infrared spectroscopy. They were further functionalized as immune labels of *E. coli* O157:H7 for a sandwich-type immune reaction between this bacterium and magnetic nanoparticles (Fe_3O_4@SiO_2). Next, the *E. coli* O157:H7 cells were captured, magnetically separated, and quantified based on the fluorescence intensity of the fluorescein released from the biolabels of the fluorescein-enriched hollow silica nanospheres. This analytic process can be completed within 75 min, and the biosensor showed a linear relationship ranging from 4 to 4.0×10^8 cfu/mL with a detection limit of 3 cfu/mL. These results show that the developed fluorescent sensor has excellent specificity, and good reproducibility and stability. This study used real spiked samples for detection, indicating that this technique has a wide range of potential applications and may be readily adapted for detecting other pathogens.

1. Introduction

The detection of pathogenic bacteria is vital for food safety, clinical diagnosis, potable water, and strategies for combating bioterrorism agents. Among the various bacterial pathogens, *Escherichia coli* O157:H7 (*E. coli* O157:H7) is one of the most dangerous types, causing serious illnesses such as hemorrhagic colitis and hemolytic uremic syndrome, especially in young and immunocompromised individuals (Zhu et al., 2011). Although significant improvements in disinfection techniques have been achieved in both the food manufacturing industry and the agricultural industry, the control of *E. coli* O157:H7 remains a problem (Laster et al., 2012). Taking ground beef as an example, it has been stated that the presence of *E. coli* O157:H7 at 1 colony forming unit (cfu)/25 g or above constitutes a significant health risk, especially because of the strong progenitive ability of *E. coli* O157:H7 (Hassan et al., 2015). Therefore, rapid and sensitive monitoring of *E. coli* O157:H7 is essential for ensuring food and water safety, and for carrying out timely and accurate disease diagnosis and treatment (Chan et al., 2013).

Traditional methods used to detect trace amounts of *E. coli* O157:H7 require amplification of the bacteria in a sample. These methods tend to be laborious, time consuming, and expensive, and require highly trained personnel, thereby delaying the results and making timely prevention of epidemic outbreaks difficult (Luo et al., 2013; Su et al., 2012). Therefore, it is extremely important to develop new techniques for the rapid and sensitive detection of *E. coli* O157:H7 to prevent catastrophic outbreaks of disease caused by public consumption of contaminated food. Fluorescent biosensor technologies are playing an increasingly important role in the detection of *E. coli* O157:H7; they have great potential to satisfy the practical need for rapid, portable, easy to use, sensitive, and

* Corresponding author.
** Corresponding author at: College of Biological, Chemical Sciences and Engineering, Jiaxing University, Jiaxing City 314001, Zhejiang Province, PR China.
E-mail addresses: yinzhengzhi@mail.zjxu.edu.cn (Z.-Z. Yin), lei.li@mail.zjxu.edu.cn (L. Li).

http://dx.doi.org/10.1016/j.bios.2015.11.018
0956-5663/

low-cost detection. In recent years, signal amplification has been verified as an efficient strategy to improve the sensitivity of these biosensors. This can be achieved by loading a large amount of probe onto the nanomaterial as a composite label (Chunglok et al., 2011; Oaew et al., 2012; Song et al., 2014; Wen et al., 2014; Zhan et al., 2014; Zhang et al., 2015). Zhan et al. (2014) successfully developed an enhanced enzyme-linked immunosorbent assay for respiratory syncytial virus by incorporating gold nanoparticles as carriers of the signaling antibody. The detection limit of this approach was 50-fold lower than for the conventional horseradish peroxidase-based immunoassay. The high sensitivity of this probe resulted from the large amount of enzyme that was loaded onto the gold nanoparticle surfaces (Zhan et al., 2014). However, the natural enzyme assembled on the nano-carrier created a bottleneck because of its limited stability, high cost, and sensitivity to the matrix, as well as difficulties in storage and transport (Wu et al., 2015). Fluorescent dyes are more stable than natural enzymes, and can be measured directly. However, low sensitivity is still a major limitation of fluorescent dyes because of the need for colorimetric detection (Wu et al., 2015). Thus, it is still necessary to develop highly sensitive, easily implementable biosensors that can be used in fluorescent dye-signal amplification strategies for the onsite detection of pathogens in complex matrices.

In this study, we report a new and simple fluorescent method for detecting *E. coli* O157:H7. Thousands of fluorescein molecules were encapsulated in protective hollow silica nanospheres (HSNs) and were used as labels for a biosensor, which provided a highly amplified and reproducible signal for fluorescence-based bioanalysis. Compared with conventional immunoassays, in where one antibody molecule is linked to only a few dye molecules, the bioconjugated HSNs enable significant amplification of the analytical signal because a large number of dye molecules are encapsulated in the individual HSN. Next, *E. coli* O157:H7 bacterial cells were captured in a one-step process and enriched using magnetic nanoparticles (MNPs). These constitute an ideal platform candidate that eliminates the need for pretreatment with amplification steps and removes matrix effects from samples, resulting in fluorescein-enriched HSNs (FHSNs) (Scheme 1). This straightforward assay results in rapid detection times, and has high sensitivity and specificity for detecting *E. coli* O157:H7. The use of HSNs as a multi-signaling molecule carrier offers enhanced detection of *E. coli* O157:H7 compared with other signal amplification systems, and can be easily adapted for the detection of other pathogens.

2. Materials and methods

2.1. Preparation of hollow silica nanospheres

First, silica nanospheres were prepared following previously established methodology (Yu et al., 2011), which involved ammonia-catalyzed hydrolysis and condensation of TEOS in an aqueous ethanol solution. Second, 1 g of CTAB was dissolved in a mixture of 100 mL of water and 70 mL of ethanol, and then 2 mL of $NH_3 \cdot H_2O$ and 1 mL of TEOS were added while stirring. The reaction was carried out at 35 °C for 6 h. The prepared silica nanospheres were centrifuged and washed with deionized water and ethanol several times. Extraction with CTAB was carried out according to the methods outlined by previous studies (Yu et al., 2011).

Next, 0.1 g of the newly prepared silica nanopheres were

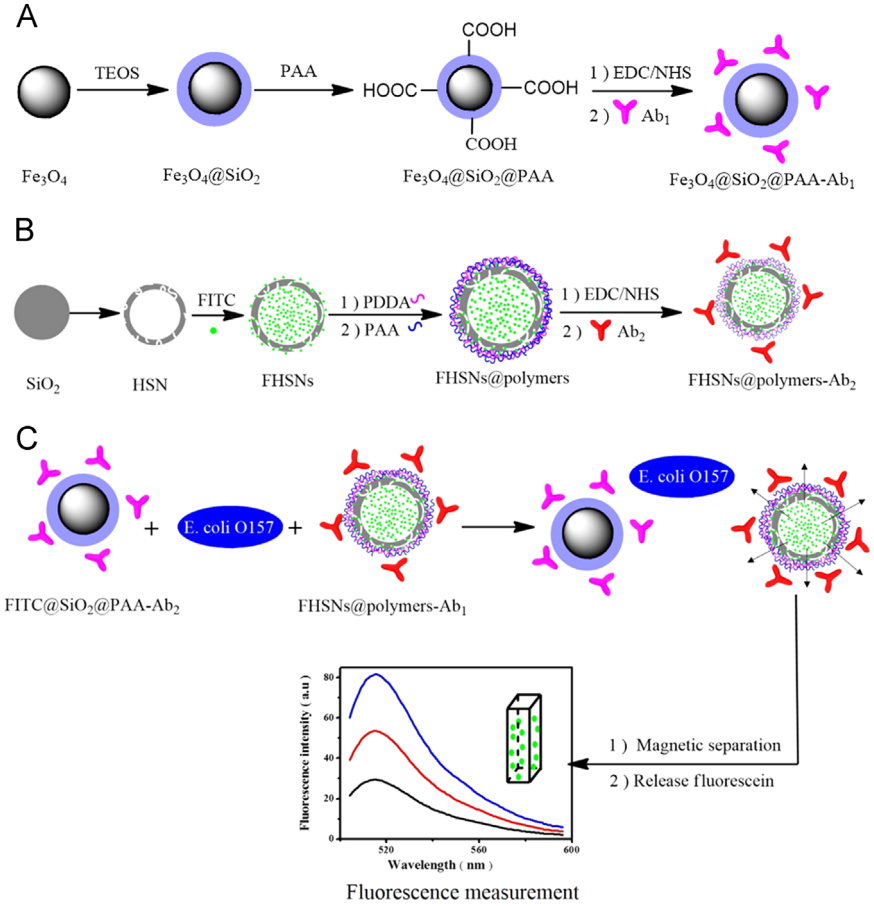

Scheme 1. Schematic of (A) the preparation of magnetic immune probes, (B) the preparation of FHSNs@polymer-Ab_2, and (C) the bioassay procedure for *E. coli* O157:H7.

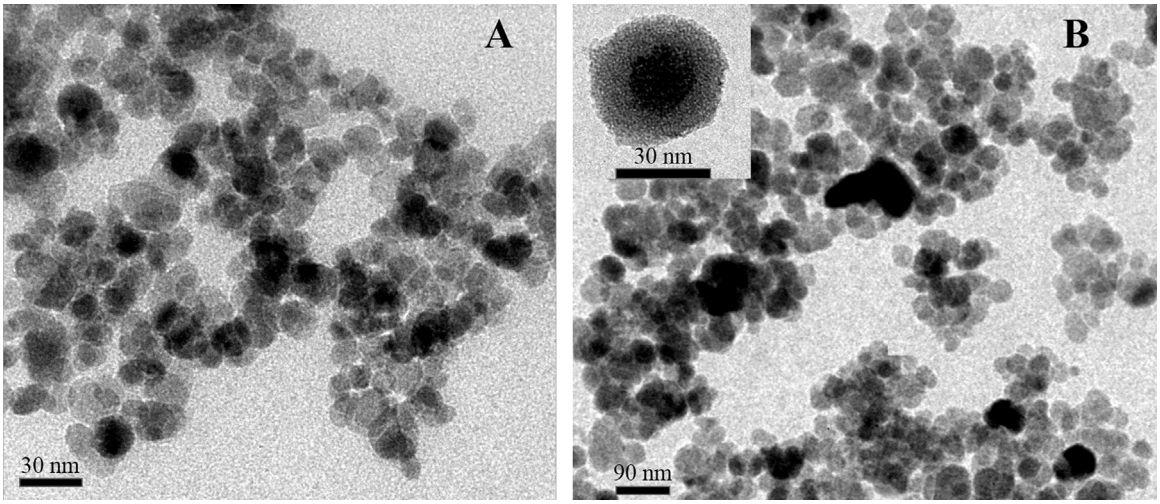

Fig. 1. TEM images of (A) Fe_3O_4 and (B) Fe_3O_4@SiO_2.

dispersed into 40 mL of hydrochloric acid solution (pH – 3.0). The mixture was stirred at room temperature for 24 h, and then transferred into a sealed Teflon-lined autoclave and heated at 180 °C for 7 h. For a slightly acidic preparation, the acid-treated dispersion was centrifuged, washed with water, then dispersed into 70 mL of hydrochloric acid solution (pH 5–6), and finally hydrothermally treated at 180 °C for 3 h. Next, the mixture was centrifuged and washed with water three times. The products were dried at 100 °C and calcined at 550 °C for 6 h to remove the CTAB, resulting in HSNs.

2.2. Preparation of immunolabels of FHSNs@polymers-Ab_2

To prepare the immunolabels, 0.05 g of HSNs and 0.012 g of fluorescein 5(6)-isothiocyanate (FITC) were dispersed into 5 mL of water. The mixture was agitated at room temperature for 48 h, after which the composites were centrifuged and dried at 40 °C. Next, 10 mg of FHSNs were dispersed into a 0.20% PDDA aqueous solution and the resulting dispersion was agitated for 30 min to yield a homogeneous suspension. The composites were centrifuged and washed with water to remove the residual PDDA, and subsequently dispersed into a 0.50% PAA solution under agitation for 30 min (Cui et al., 2008). The residual PAA polymer was removed using high-speed centrifugation. The resulting nanospheres were further self-assembled by PDDA and PAA by repeating the steps above. The final nanocomposites (FHSNs@polymers) were able to protect the inner fluorescein dye molecule to prevent leakage; this property was verified by analyzing the ultraviolet absorption and fluorescence spectra of the supernatant after centrifugation. The amount of fluorescein stored in the FHSNs@polymers was determined by dissolving 10 mg of FHSNs and detecting the amount of released fluorescein. Multiple detections obtained the same content of 16.94%.

After layer-by-layer self-assembly, the obtained nanospheres were immersed in a solution that contained 1 mg/mL EDC and 0.5 mg/mL NHS for 30 min to activate the carboxyl group of the PAA layer (Viswanathan et al., 2012). Afterwards, the nanospheres were immediately immersed in a mixture of 0.2 mg/mL Ab_2 solution for 2 h to yield immunolabels of FHSNs@polymers-Ab_2. After discarding the supernatant by centrifugation, the mixture was washed three times with PBS to remove residual antibodies. The remnant active sites of the FHSNs@polymers-Ab_2 were blocked with PBS containing 5% bovine serum albumin at 37 °C for 2 h. Finally, the nanocomposites were separated and washed with PBS (pH 7.4) three times, and stored in pH 7.4 PBS at 4 °C.

2.3. Bioassay procedure for *E. coli* O157:H7

As shown in Schemes 1C, 0.1 mL of Fe_3O_4@SiO_2@PAA-Ab_1 and 1.0 mL of FHSNs@polymers-Ab_2 were added to a PBS solution (1.0 mL) containing *E. coli* O157:H7. The mixture was vigorously shaken on a thermostatic shaker at 37 °C for 60 min. The mixture was magnetically treated, and the non-magnetic mixture was discarded. The magnetically separated complexes were carefully washed with PBS five times. Next, 3 mL of 0.1 mol/mL sodium hydroxide solution were added for 10 min under ultrasound treatment, which dissolved the HSNs and released the internal fluorescence. The solution was adjusted to pH 10 and the fluorescence intensity was recorded to determine the *E. coli* O157:H7 content.

3. Results and discussion

3.1. Characterization of magnetic beads and fluorescent silica

TEM images of Fe_3O_4 and Fe_3O_4@SiO_2 are shown in Fig. 1. Fe_3O_4 displayed angular and amorphous particles with sizes ranging from 7 to 20 nm. The apparent aggregation of Fe_3O_4 observed in the TEM image could result from its strong magnetic properties. Compared with Fe_3O_4, most of the Fe_3O_4@SiO_2 particles were quasi-spherical with larger diameters ranging from 30 to 50 nm; the particles were also separated from each other, possibly owing to their weakened magnetic properties and the mutual repulsion of their surface functional groups (Fig. 1B).

Fig. S1 A shows the FTIR of Fe_3O_4, Fe_3O_4@SiO_2, and Fe_3O_4@SiO_2@PAA. Fe_3O_4 exhibited one characteristic peak at approximately 652 cm^{-1} (curve a), which corresponds to the Fe–O stretching vibration. As shown in curve b, SiO_2 exhibited one characteristic peak at approximately 1092 cm^{-1}, which corresponds to the Si–O–Si stretching vibration. The peak at 956 cm^{-1} is due to the Si–OH groups. After the introduction of PAA, the peak intensity at 1663 cm^{-1} for the C=C group increased significantly (Li et al., 2015). The peak at approximately 1379 cm^{-1} results from O–H deformation stretching vibration of the C–OH group, and the new peaks at 2925 cm^{-1} can be ascribed to asymmetric stretching of the $–CH_2–$ group (Du et al., 2013). The FTIR spectra and the peak at 1092 cm^{-1} decreased. The existence of these peaks confirms the successful preparation of Fe_3O_4@SiO_2@PAA.

The X-ray diffraction patterns of Fe_3O_4, Fe_3O_4@SiO_2 and Fe_3O_4@SiO_2@PAA are shown in Fig. S1B. Compared with Fe_3O_4, the

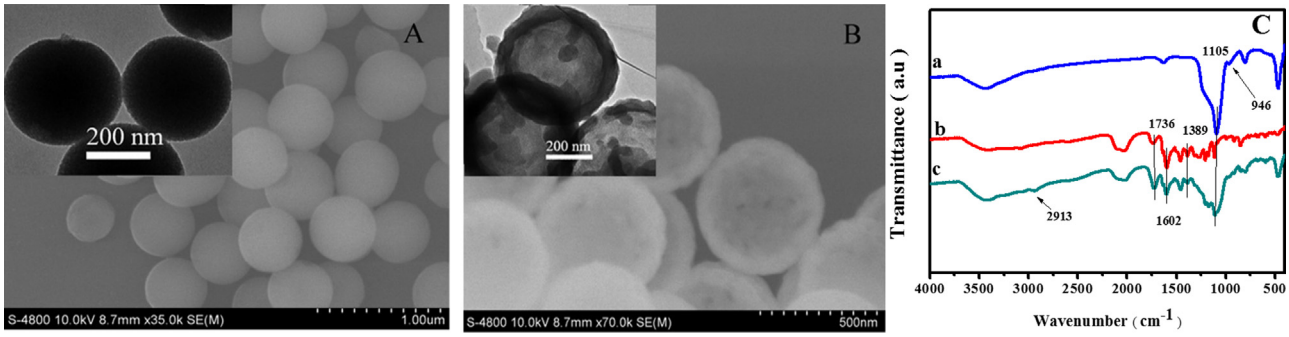

Fig. 2. Characterization of the nanospheres, HSNs, and FHSN@polymer using SEM, TEM, and FTIR. SEM and TEM (insert) images of (A) SiO_2 nanospheres and (B) FHSNs@polymer; (C) FTIR of (a) HSNs, (b) FITC, and (c) FHSNs@polymers.

diffraction peaks of Fe_3O_4@SiO_2 and Fe_3O_4@SiO_2@PAA exhibited just one characteristic peak at $2\theta=22°$. This result confirms that SiO_2 was successfully grafted onto the Fe_3O_4 surface. The magnetic properties of the Fe_3O_4 nanoparticles, Fe_3O_4@SiO_2, and Fe_3O_4@SiO_2@PAA were characterized using a vibrating sample magnetometer at room temperature, and the results are shown in Fig. S1C. The saturation magnetization value for Fe_3O_4 was 70.299 emu g^{-1}, smaller than that of the theoretical specific saturation magnetization of bulk magnetite (Zaitsev et al., 1999). This decrease is likely caused by the small particle surface effect. The saturation magnetization values of Fe_3O_4@SiO_2 (18.104 emu g^{-1}) and Fe_3O_4@SiO_2@PAA (18.097 emu g^{-1}) were far lower than values for pure Fe_3O_4 nanoparticles. This decrease can most likely be attributed to the existence of silica shells on the surface of Fe_3O_4 nanoparticles, leading to a weakening of their magnetic properties.

The SEM and TEM images show that the SiO_2 nanospheres have round, uniform structures with flat surfaces and an average diameter of 300 nm (Fig. 2A). Fig. 2B demonstrates the contrast between the core and the shell of the sphere indicating the hollow structure of the HSNs with an average diameter of 350 nm and a shell thickness of approximately 25 nm. We note that the surface structure of the HSNs is uneven and blurry compared with bare SiO_2 nanospheres on account of their surface functionalization. The unique structure and surface features of HSNs make them attractive candidates for dye molecule storage purposes. Fig. 2C shows the FTIR of HSNs, FITC, and FHSNs@polymers. The HSNs exhibited one characteristic peak at approximately 1105 cm^{-1} (curve a), which corresponds to the Si–O–Si stretching vibration, and the peak at 946 cm^{-1} corresponds to the Si–O–H groups. After the enrichment of FITC molecules and the introduction of PDDA and PAA, the absorption peaks became more complex. A sharp peak at 1736 cm^{-1} can be attributed to the C=O stretch vibration. The peak intensity of 1602 cm^{-1} for the C=C group increased significantly and the peak of 1105 cm^{-1} decreased. The peak at approximately 1389 cm^{-1} results from O–H deformation and stretching vibration of the C–O–H group. These results further confirm that FHSNs@polymers were successfully obtained following enrichment with FITC and layer-by-layer self-assembly of polymers.

3.2. Optimization of the detection conditions

The acidity of the fluorescein-release solution used to release FHSN labels from immuno-complexes was vital to the performance of the biosensor. In acidic and neutral environments, the dye molecules were protected by an undissolved SiO_2 shell and shrink polymer layers, and no fluorescein leaked. In an alkaline solution of sodium hydroxide, the weaker the alkalinity, the longer the time that was needed to release all dye molecules. Furthermore, the fluorescent intensity of the released fluorescein was affected by the acidity, as shown in Fig. S2A; this property could be because of the structure of FITC. Taking both of these factors into account, 0.1 mol/mL of sodium hydroxide was selected for release of the fluorescein, and a solution of pH 10.0 was used as the detection medium.

Incubation temperature and incubation time were important factors for the immunological reaction. The effect of incubation time, ranging from 10 to 100 min, on fluorescence intensity was assessed for the immunoreaction labels (Fig. S2B). The experimental results showed that the intensity of fluorescence increased with incubation time, and reached a constant value after 60 min. A longer incubation time did not improve the intensity of the labeled fluorescence. Therefore, 60 min was selected as the incubation time for the reaction. Investigating the effect of incubation temperatures showed that the maximum signal occurred at 37 °C (Fig. S2C). When the incubation temperature was higher than 37 °C, the intensity of the fluorescence decreased, which could be because of a reduction in biomolecule activity at high temperatures (Chiu et al., 2013). Thus, an incubation temperature of 37 °C was chosen for the analysis of *E. coli* O157:H7 using an FHSN-labeled antibody.

3.3. Analytical performance

After determining that the developed fluorescent biosensor could sensitively detect target *E. coli* O157:H7, we tested the ability of the biosensor to detect different concentrations of *E. coli* O157:H7. As shown in Fig. 3A, the fluorescent signal gradually increased with *E. coli* O157:H7 concentration and showed a good linear relationship with the *E. coli* O157:H7 concentration from 4 to 4×10^8 cfu/mL. This indicated that the *E. coli* O157:H7 concentration could be quantitatively measured by the fluorescent signal using the regression equation $y=10.2367\times+25.52054$, a detection limit of 3 cfu/mL (estimated using 3 s, where s is the relative standard deviation of a blank solution), and a correlation coefficient of 0.9913.

Studies over the past 10 years have detected *E. coli* O157:H7 using electroanalysis, electrochemical impedance spectroscopy, electrophoresis, quartz crystal microbalance, direct-charge transfer, giant magnetoimpedance, surface plasmon resonance, surface enhanced Raman spectroscopy, electrochemiluminescence, chemiluminescence, colorimetric analysis, and fluorescence. We compared our findings with the results of previous studies using well-known technical indicators for analytical methods: the limit of detection, the linear interval, the detection period, and the anti-interference ability (Table S1). The limit of detection for the biosensor developed in this study was lower than any previously reported by studies using different analytical technologies. This result indicates that FHSNs act as excellent biolabels in our assay system. The linear interval in our system was also wider than any

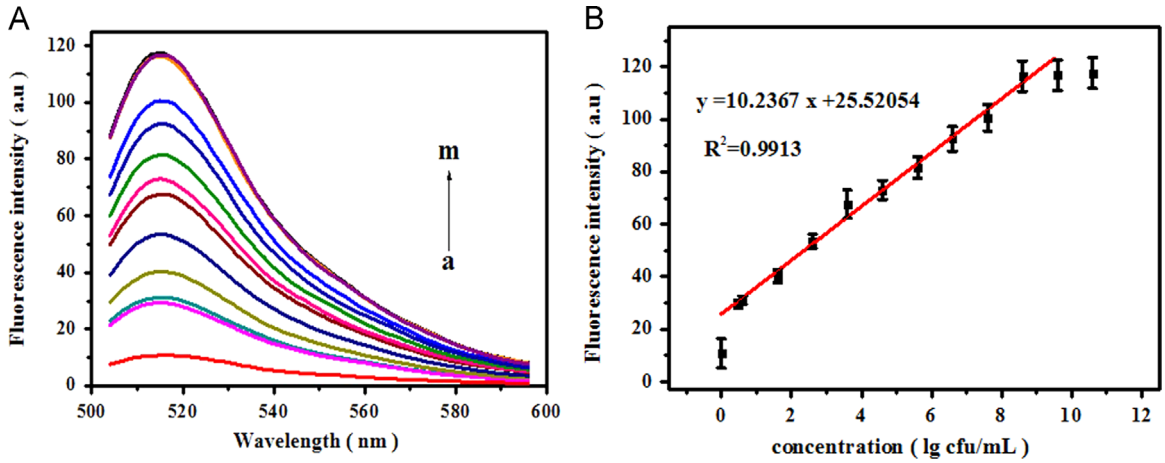

Fig. 3. Characterization of the fluorescent responses of released FHSNs from the biosensor using different concentrations of *E. coli* O157:H7. (A) Fluorescent responses of released FHSNs from the biosensor using different concentrations of *E. coli* O157:H7. (a): 0 cfu/mL, (b): 3 cfu/mL, (c): 4 cfu/mL, (d): 4×10^1 cfu/mL, (e): 4×10^2 cfu/mL, (f): 4×10^3 cfu/mL, (g): 4×10^4 cfu/mL, (h): 4×10^5 cfu/mL, (i): 4×10^6 cfu/mL, (j): 4×10^7 cfu/mL, (k): 4×10^8 cfu/mL, (l): 4×10^9 cfu/mL, and (m): 4×10^{10} cfu/mL). (B) The corresponding calibration curve between fluorescent values of released FHSNs and the concentration of *E. coli* O157:H7 ($\lambda_{em,max}$: 515 nm, and other assay conditions were optimized).

previously reported values. The total assay time for our system of 75 min (60 min for immunomagnetic separation, and 15 min for release and measurement) was also comparable to the results of previous studies. This result indicates that MNPs are highly efficient for separation and enrichment in the assay system. Together, our findings confirm that the proposed biosensor can sensitively detect *E. coli* O157:H7 over a wide linear range and in a short detection period. Thus, our study demonstrates the significance of amplification of FHSN nanocomposites and the role of MNPs in separation and enrichment.

Fig. S3a shows a typical fluorescence microscopy image of immune complexes using fluorescein-free labels. No fluorescence emission was observed in this case or from FHSNs not labeled with an antibody (Fig. S3b), Fe_3O_4@SiO_2@PAA not labeled with an antibody (Fig. S3c), or the magnetic separation product from the immune mixture in the absence of *E. coli* O157:H7 (Fig. S3d). However, an obvious green fluorescent signal was observed from immune complexes using FHSN labels, indicating that the fluorescence was from FHSNs, which were magnetically separated via an immune reaction on the surface of *E. coli* O157:H7. Thus, our FHSNs produced a fluorescence response only in the presence of both target *E. coli* O157:H7 and magnetic probes, leading to high specificity, which suggests that nonspecific adsorption was negligible. These experimental results confirm that the prepared FHSN conjugation could be used as a label for bioassay applications.

3.4. Specificity, reproducibility, and stability of the immunosensor

To investigate the specificity of the proposed immunoassay, we tested different pathogens in our system (*E. coli* O157:H7, *Staphylococcus aureus*, *E. coli* ATCC 8739, and a mixture of *S. aureus*, *E. coli* O157:H7, and *E. coli* ATCC 8739). The prepared magnetic probes and immune FHSNs were mixed with a solution of the test organism, followed by magnetic separation, fluorescence release, and fluorescent analysis, and the results are shown in Fig. S4. In the absence of *E. coli* O157:H7, negligible weak fluorescent signals were recorded; these can probably be attributed to the surface complexity of *S. aureus* or *E. coli*, including phagocytosis. However, for samples containing *E. coli* O157:H7 alone or in a mixture, the response signal increased dramatically. These results clearly demonstrate that the proposed immunoassay is *E. coli* O157:H7-specific with high selectivity.

The stability of the immunosensor was studied as follows. After the bio-conjugated FHSNs were stored at 4 °C for 60 days, the fluorescent intensity of the released fluorescence showed an obvious change compared with the initial fluorescence intensity, confirming that no leakage had occurred. Furthermore, when the bio-conjugated FHSNs that had been stored at 4 °C for 60 days were used in the same analytical system with newly prepared magnetic probes, 98.9% of its initial response to *E. coli* O157:H7 was retained with high specificity. When magnetic probes that had been stored at 4 °C for 60 days were used in the analytical system with newly prepared bio-conjugated FHSNs, 98.2% of its initial response to *E. coli* O157:H7 was retained, likely owing to the intrinsic magnetism and the surface-modified layer of the magnetic probes. When the bio-conjugated FHSNs and magnetic probes were used after storage at 4 °C for 60 days, the fluorescence signal retained more than 96.7% of its initial response to *E. coli* O157:H7 with satisfactory specificity. These results indicated that the bio-conjugate FHSNs and magnetic probes have good stability and excellent specificity, which can be attributed to the well-known biocompatibility of the surface microenvironment for antibody conjugation.

3.5. Real sample analysis

The reliability of the system was further evaluated by recovery experiments using real samples. *E. coli* O157:H7 was detected in spiked samples, i.e., commercially obtained milk, orange juice, and river water, four typical coli forms (*E. coli* O91, *E. coli* O97, *E. coli* O100, *E. coli* O149) and a mixture of the coliforms using the method described above (Table 1). The results ranged from 90.47% to 117.32%, higher levels than observed with a chemiluminescence assay (90–120%) (Magliulo et al., 2007) or a bioluminescence assay ($75.49 \pm 15.48\%$) (Guan et al., 2010). This high level of recovery can be explained by the excellent specific recognition of immune labels and the efficient separation by MNPs, which can reduce the external interference signal. These results confirm that this method is applicable for the detection of *E. coli* O157:H7 in real samples.

4. Conclusion

In this study, we developed a highly sensitive and efficient fluorescent immunoassay strategy for the rapid detection of *E. coli*

Table 1
Levels of recovery with *E. coli* O157:H7-spiked real samples. Every sample was detected three times, and recovery is expressed as the ratio of the number of cfu/mL detected/number of cfu/mL added.

Sample number	Added (cfu/mL)	Detected (cfu/mL)	RSD (%)	Recovery (%)
Milk 1	4×10^1	4.03×10^1	3.94	100.85
Milk 2	4×10^2	3.97×10^2	3.67	99.14
Milk 3	4×10^3	4.10×10^3	3.37	102.61
Water 1	4×10^1	3.81×10^1	1.36	95.17
Water 2	4×10^2	3.90×10^2	2.75	97.55
Water 3	4×10^3	4.33×10^3	2.40	108.20
Orange juice 1	4×10^1	3.61×10^1	3.12	90.21
Orange juice 2	4×10^2	4.08×10^2	2.39	102.05
Orange juice 3	4×10^3	4.13×10^3	3.15	103.31
Sample 1	4×10^3	4.27×10^3	2.64	106.81
Sample 2	4×10^3	4.31×10^3	3.92	107.71
Sample 3	4×10^3	4.41×10^3	3.34	110.55
Sample 4	4×10^3	4.21×10^3	3.8	105.20
Sample 5	4×10^3	4.70×10^3	1.50	117.32

RSD, relative standard deviation.
Sample 1: 4×10^3 cfu/mL of *E. coli* O91.
Sample 2: 4×10^3 cfu/mL of *E. coli* O97.
Sample 3: 4×10^3 cfu/mL of *E. coli* O100.
Sample 4: 4×10^3 cfu/mL of *E. coli* O149.
Sample 5: a mixture of *E. coli* O91 (1×10^3 cfu/mL), *E. coli* O97 (1×10^3 cfu/mL), *E. coli* O100 (1×10^3 cfu/mL) and *E. coli* O149 (1×10^3 cfu/mL).

O157:H7; the method uses FHSNs as biolabels and incorporates a magnetic concentration step. The prepared bio-conjugated FHSNs have fine fluorescein-release properties, high stability, and good biocompatibility for detecting *E. coli* O157:H7. The biosensor has a linear relationship from 4 to 4.0×10^8 cfu/mL with a limit of detection of 3 cfu/mL, and the analytic process can be completed within 75 min. The high complexity of the real samples tested, including milk, orange juice, and river water, suggests that this method could have wide-reaching applications in clinical diagnosis, environmental monitoring, and food security. The possibility of avoiding enrichment, together with the use of a portable handheld potentiostat paired with a pocket PC enables rapid field analysis of food and water samples without requiring highly equipped and specialized laboratories. Moreover, this methodology could be readily adapted for detecting other pathogens by using different bacterium-specific bioelements.

Acknowledgment

We appreciate financial support from the Foundation of the Program for Science and Technology of Zhejiang Province (2013C32038, 2015C32067), the National Natural Science Foundation of China (21177049), the Natural Science Foundation of Zhejiang Province (LQ12B05005, LQ14B050002), the State Key Laboratory of Analytical Chemistry for Life Science (SKLACLS1205), the Open Research Fund of Top Key Discipline of Chemistry in Zhejiang Provincial Colleges and Key Laboratory of the Ministry of Education for Advanced Catalysis Materials (Zhejiang Normal University ZJHX201502).

Appendix A. Supplementary material

Supplementary data associated with this article can be found in the online version at http://dx.doi.org/10.1016/j.bios.2015.11.018.

References

Chan, K.Y., Ye, W.W., Zhang, Y., Xiao, L.D., Leung, P.H., Li, Y., Yang, M., 2013. Ultrasensitive detection of *E. coli* O157:H7 with biofunctional magnetic bead concentration via nanoporous membrane based electrochemical immunosensor. Biosens. Bioelectron. 41, 532–537.
Chiu, Y.F., Huang, C.K., Shigeto, S., 2013. In vivo probing of the temperature responses of intracellular biomolecules in yeast cells by label-free Raman microspectroscopy. Chembiochem.: Eur. J. Chem. Biol. 14 (8), 1001–1005.
Chunglok, W., Wuragil, D.K., Oaew, S., Somasundrum, M., Surareungchai, W., 2011. Immunoassay based on carbon nanotubes-enhanced ELISA for Salmonella enterica serovar Typhimurium. Biosens. Bioelectron. 26 (8), 3584–3589.
Cui, R., Liu, C., Shen, J., Gao, D., Zhu, J.-J., Chen, H.-Y., 2008. Gold nanoparticle-colloidal carbon nanosphere hybrid material: preparation, characterization, and application for an amplified electrochemical immunoassay. Adv. Funct. Mater. 18 (15), 2197–2204.
Du, Y., Du, Z., Zou, W., Li, H., Mi, J., Zhang, C., 2013. Carbon dioxide adsorbent based on rich amines loaded nano-silica. J. Colloid Interface Sci. 409, 123–128.
Guan, X., Zhang, H.J., Bi, Y.N., Zhang, L., Hao, D.L., 2010. Rapid detection of pathogens using antibody-coated microbeads with bioluminescence in microfluidic chips. Biomed. Microdevices 12 (4), 683–691.
Hassan, A.-R.H.A.-A., de la Escosura-Muñiz, A., Merkoçi, A., 2015. Highly sensitive and rapid determination of *Escherichia coli* O157: H7 in minced beef and water using electrocatalytic gold nanoparticle tags. Biosens. Bioelectron. 67, 511–515.
Laster, B.A., Harris, K.B., Lucia, L.M., Castillo, A., Savell, J.W., 2012. Efficacy of trimming chilled beef during fabrication to control *Escherichia coli* O157:H7 surrogates on subsequent subprimals. Meat Sci. 90 (2), 420–425.
Li, J., Li, Q., Zeng, Y., Tang, T., Pan, Y., Li, L., 2015. An electrochemical sensor for the sensitive determination of phenylethanolamine A based on a novel composite of reduced graphene oxide and poly (ionic liquid). RSC Adv. 5 (1), 717–725.
Luo, C., Tang, H., Cheng, W., Yan, L., Zhang, D., Ju, H., Ding, S., 2013. A sensitive electrochemical DNA biosensor for specific detection of Enterobacteriaceae bacteria by exonuclease III-assisted signal amplification. Biosens. Bioelectron. 48, 132–137.
Magliulo, M., Simoni, P., Guardigli, M., Michelini, E., Luciani, M., Lelli, R., Roda, A., 2007. A rapid multiplexed chemiluminescent immunoassay for the detection of *Escherichia coli* O157: H7, *Yersinia enterocolitica*, *Salmonella typhimurium*, and Listeria monocytogenes pathogen bacteria. J. Agric. Food Chem. 55 (13), 4933–4939.
Oaew, S., Charlermroj, R., Pattarakankul, T., Karoonuthaisiri, N., 2012. Gold nanoparticles/horseradish peroxidase encapsulated polyelectrolyte nanocapsule for signal amplification in Listeria monocytogenes detection. Biosens. Bioelectron. 34 (1), 238–243.
Song, E., Han, W., Li, J., Jiang, Y., Cheng, D., Song, Y., Zhang, P., Tan, W., 2014. Magnetic-encoded fluorescent multifunctional nanospheres for simultaneous multicomponent analysis. Anal. Chem. 86 (19), 9434–9442.
Su, H., Ma, Q., Shang, K., Liu, T., Yin, H., Ai, S., 2012. Gold nanoparticles as colorimetric sensor: a case study on *E. coli* O157:H7 as a model for Gram-negative bacteria. Sens. Actuators B: Chem. 161 (1), 298–303.
Viswanathan, S., Rani, C., Ho, J.A., 2012. Electrochemical immunosensor for multiplexed detection of food-borne pathogens using nanocrystal bioconjugates and MWCNT screen-printed electrode. Talanta 94, 315–319.
Wen, J., Zhou, S., Yuan, Y., 2014. Graphene oxide as nanogold carrier for ultrasensitive electrochemical immunoassay of *Shewanella oneidensis* with silver enhancement strategy. Biosens. Bioelectron. 52, 44–49.
Wu, W., Zhao, S., Mao, Y., Fang, Z., Lu, X., Zeng, L., 2015. A sensitive lateral flow biosensor for *Escherichia coli* O157:H7 detection based on aptamer mediated strand displacement amplification. Anal. Chim. Acta 861, 62–68.
Yu, Q., Wang, P., Hu, S., Hui, J., Zhuang, J., Wang, X., 2011. Hydrothermal synthesis of hollow silica spheres under acidic conditions. Langmuir: ACS J. Surf. Colloid. 27 (11), 7185–7191.
Zaitsev, V.S., Filimonov, D.S., Presnyakov, I.A., Gambino, R.J., Chu, B., 1999. Physical and chemical properties of magnetite and magnetite-polymer nanoparticles and their colloidal dispersions. J. Colloid Interface Sci. 212 (1), 49–57.
Zhan, L., Wu, W.B., Yang, X.X., Huang, C.Z., 2014. Gold nanoparticle-based enhanced ELISA for respiratory syncytial virus. New J. Chem. 38 (7), 2935.
Zhang, H., Zhang, Y., Lin, Y., Liang, T., Chen, Z., Li, J., Yue, Z., Lv, J., Jiang, Q., Yi, C., 2015. Ultrasensitive detection and rapid identification of multiple foodborne pathogens with the naked eyes. Biosens. Bioelectron. 71, 186–193.
Zhu, P., Shelton, D.R., Li, S., Adams, D.L., Karns, J.S., Amstutz, P., Tang, C.M., 2011. Detection of E. coli O157:H7 by immunomagnetic separation coupled with fluorescence immunoassay. Biosens. Bioelectron. 30 (1), 337–341.